Applied Catalysis B: Environmental 324 (2023) 122286

Contents lists available at ScienceDirect

Applied Catalysis B: Environmental

journal homepage: www.elsevier.com/locate/apcatb

Aldol condensation of acetaldehyde for butanol synthesis: A temporal analysis of products study

Joachim Pasel [a,*], Johannes Häusler [a], Dirk Schmitt [a], Helen Valencia [b,c], Joachim Mayer [b,c], Ralf Peters [a]

[a] Institute of Energy and Climate Research, IEK-14: Electrochemical Process Engineering, Forschungszentrum Jülich GmbH, 52425 Jülich, Germany
[b] Central Facility for Electron Microscopy (GFE), RWTH Aachen University, 52074 Aachen, Germany
[c] Ernst Ruska-Centre (ER-C) for Microscopy and Spectroscopy with Electrons, Forschungszentrum Jülich GmbH, 52425 Jülich, Germany

ARTICLE INFO

Keywords:
Renewable fuels
Aldol condensation
Guerbet reaction
Lanthanide oxides
Temporal analysis of products

ABSTRACT

The catalytic upgrading of CO_2-based ethanol into valuable products, such as higher alcohols, is of increasing interest. Carbon-neutral n-butanol can substitute major fractions of conventional gasoline in the transport sector of the future. A promising synthesis path towards n-butanol is the Guerbet reaction, in which the homo aldol condensation of acetaldehyde constitutes an important intermediate step, which was investigated using the Temporal Analysis of Products methodology. This investigation employed the lanthanide oxides Dy_2O_3, Eu_2O_3, and Er_2O_3, supported on activated carbon due to their varying basic characteristics. In addition to the aldol condensation of acetaldehyde yielding butanol, its decomposition into CO, CH_4, and H_2 also occurred. Furthermore, acetaldehyde pulsing onto the catalyst surface of Dy_2O_3/C also lead to the formation of carbonaceous deposits. Fortunately, catalyst regeneration by means of O_2 pulsing was successful. Other reaction routes yielding acidic acid, ethyl acetate, or diethyl ether could be experimentally excluded.

1. Introduction

Although the electrification of the power train of passenger cars via batteries and electric motors will most likely strongly increase in the coming years (fostered by favorable political conditions, etc.), huge volumetric demands for green and sustainable fuels for the transport sector will persist wherever heavy masses must be transported over long distances ("hard to decarbonize sectors"). In this respect, n-butanol possesses all of the necessary physical and chemical properties to substitute gasoline in the fuel spectrum to a considerable extent. These are density, viscosity, solubility in water, lower heating value, boiling point, flash point, self-ignition temperature, motor octane number, etc. Its production can be achieved via the Guerbet reaction depicted below in Fig. 1. This reaction sequence starts with ethanol, which can be considered sustainable, when it is, e.g., produced via the homologation of green methanol. The latter can be generated from H_2 and CO_2, where wind- or solar-driven water electrolysis facilities and CO_2 from the exhausts of, e.g., steelworks are available in necessary quantities.

In Fig. 1, first two moles of ethanol are dehydrogenated, giving two moles of H_2 and two of acetaldehyde, which further react to form 3-hydroxy-butanal in an aldol condensation step. This intermediate product, in turn, further splits off H_2O to form crotonaldehyde and, after re-hydrogenation, 1-butanol.

In the literature, there are two main explanatory approaches with respect to experimentally observed catalytic activities for the intermediate step of the Guerbet reaction in Fig. 1, i.e., the aldol condensation of two acetaldehyde molecules. Some authors underline that it is crucial to have a well-balanced ratio between acidic and basic sites on the catalyst surface, while others stress the importance of strong basic sites for the aldol condensation step. Against this background, the lanthanide oxides came into the focus of this paper. According to the Fajans' rules, the salts of the lanthanides show a slightly less ionic character as the radii of the Ln^{3+}-ions in these salts continuously decrease from Cer at the beginning of the lanthanide series to Luthetium at its end. A reduced ionic character of the salts in turn results in a reduction of their basic properties. That means that the lanthanide oxides become somewhat more acidic along their series while, however, remaining mainly basic [1]. For this paper, Er_2O_3 was chosen as an oxide with a more balanced ratio between acidic and basic sites on the catalyst surface, while Eu_2O_3 acts for strong basicity. Dy_2O_3 was taken as a compromise between Er_2O_3 and Eu_2O_3.

* Corresponding author.
E-mail addresses: j.pasel@fz-juelich.de (J. Pasel), gfe@gfe.rwth-aachen.de (H. Valencia), j.mayer@fz-juelich.de (J. Mayer), ra.peters@fz-juelich.de (R. Peters).

https://doi.org/10.1016/j.apcatb.2022.122286
Received 17 August 2022; Received in revised form 7 December 2022; Accepted 10 December 2022
Available online 13 December 2022

So, by choosing these three lanthanide oxides supported on activated carbon, this paper aims at shedding some light on the above-mentioned research interrogation whether strong basic properties or a balanced ratio between basic and acidic sites are more beneficial for the aldol condensation within the Guerbet reaction. In this respect, the transient Temporal Analysis of Products methodology (TAP) was applied by pulsing acetaldehyde molecules onto the surfaces of Eu_2O_3/C, Dy_2O_3/C and Er_2O_3/C, respectively. As a second focus of this paper, the use of TAP additionally targeted at improving the understanding of the single reaction steps that characterize the homo aldol condensation of acetaldehyde on Eu_2O_3/C, Dy_2O_3/C and Er_2O_3/C, respectively.

In the following, at first papers stressing the importance of strong basicity are presented in more detail. Wang et al. [2] analyzed the different functions of a $NiCeO_2$/AC catalyst. The characterization displayed a good dispersion of both the Ni and CeO_2 sites over the activated carbon support. On the one hand, the uniformly-distributed Ni particles enhanced the reduction of adsorbed ethanol, yielding acetaldehyde. On the other, the CeO_2 sites revealed that strong basic characteristics are beneficial for the aldol condensation reaction. Cimino et al. [3] investigated three different catalyst supports (hydroxyapatite, γ-Al_2O_3, MgO) and the influence of their acidic and basic characteristics on the conversion of ethanol to yield butanol. Only MgO was found to exhibit a measurable activity, which was ascribed to its high basicity. If doped with Ni or Ru, an increase in the catalytic activity was observed and explained by, on the one hand, additional basicity and, on the other, redox features of the metals favoring the hydrogenation and dehydrogenation steps of the Guerbet reaction. Comparable results were observed by Wang et al. with a Ni/MgO-catalyst [4]. Also, Ndou et al. [5] found that the MgO catalyst was the most active and selective for ethanol upgrading if compared with, e.g., CaO, BaO, or Mg/SiO_2. Leon et al. [6,7], Pang et al. [8], Ramasamy et al. [9], Zhang et al. [10,11], and Pieta et al. [12] also chose Mg-Al mixed oxides and analyzed the functions of the acidic and basic sites of the catalysts. For instance, Leon at al. found that acidic sites favored the dehydration yielding ethylene, whereas basic centers with mean strength enhanced the dehydrogenation of ethanol into acetaldehyde, with the most intense basic sites promoting the condensation reaction of acetaldehyde. Ogo et al. [13,14] used $Sr_{10}(PO_4)_6(OH)_2$-catalysts for the synthesis of n-butanol from ethanol with varying molar ratios of Sr/P. They observed that high values for this ratio (equivalent to more strong basic sites on the catalyst surface) were beneficial to the selectivity towards n-butanol, as they favored the acetaldehyde condensation step and prevented coking. Ca-based catalysts (CaC_2 and $Ca(OCH_2CH_3)_2$) were investigated by Wang et al. [15,16], Wang et al. [17] (Ca/hydroxyapatite) and Pinzón et al. [18] (Ca/Al_2O_3 and Ca-P/Al_2O_3) in the production of n-butanol and other higher alcohols from ethanol. In the case of CaC_2, the authors emphasize the strong basic nature that makes it easier to abstract an H-atom from ethanol. For $Ca(OCH_2CH_3)_2$, DFT calculations revealed some mechanistic details, e.g., that ethanol adsorbs via its O-atom on the Ca of $Ca(OCH_2CH_3)_2$, yielding the intermediate acetaldehyde. In addition to Ca, Onyestyak chose Li, Na, K, Cs, Mg, and Zn supported on activated carbon as catalysts in the Guerbet reaction [19]. He observed that the earth alkali metals with higher basicity were more active in the formation of n-butanol and a mixture of higher alcohols. In turn, Perrone et al. [20] synthesized Cu-MgAl(O)- and CuLa-MgAl(O)-catalysts for the formation of n-butanol and n-hexanol from ethanol. They found that the addition of La to Cu-MgAl(O) strongly enhanced the basicity and favored the formation of n-hexanol to the detriment of n-butanol production. The selectivity towards n-hexanol increased from 10% to 42%. A different oxidic catalyst, i.e., ZrO_2-Y_2O_3, was analyzed by Vlasenko et al. [21]. In this case, the calcination temperature was of major importance, as the most suitable one, at 500 °C, steadied the tetragonal phase of ZrO_2 with outstanding basicity.

On the contrary, hereafter some exemplary papers highlight a balanced ratio between basicity and acidity. Graphite was applied by Lopez-Olmos et al. and doped with Cu and MgO, BaO, ZnO, and MnO, respectively [22]. Amongst these catalysts, Cu-MnO/graphite showed the most promising n-butanol yield. Cu was responsible for hydrogenating and dehydrogenating, whereas the basic and acidic centers of MnO enabled the condensation reaction. Di Cosimo et al. [23,24] performed two studies on Mg_yAlO_x catalysts for the condensation of ethanol. They found that the aldol condensation of two acetaldehyde molecules to yield 1-butanol and iso-butanol is favored on Mg-rich catalysts with Al^{3+} Lewis acid sites and Mg^{2+}–O^{2-} basic pairs. Dai and Zhang [25] wrote a short review on improved materials for the C–C bond coupling of two ethanol molecules to yield valuable products such as n-butanol. They report on a Pd/Mg-AlO_x-catalyst with 72.7% selectivity towards n-butanol and even 86.4% when a Sr-P hydroxyapatite is used. The authors stress the importance of having a balanced ratio between acidic and basic sites on the catalyst. Similarly, Osman et al. [26] found in their DRIFTS study of hydroxyapatite catalysts that OH-groups and acidic species (Ca^{2+}) jointly function in the formation of acetaldehyde and its subsequent condensation into n-butanol. Meanwhile, Quesada et al. focused on Mg-Al mixed oxides as support, which were doped with Cu nanoparticles [27], Ru and Pd [28], and Co and Ni, respectively [29]. In the case of the Cu nanoparticles [27], the quantity of n-butanol produced was twelve times higher than in the case of pure Mg-Al oxide. It was found to be necessary that acid/basic centers and metallic sites be adjacent. For the Ru-doped catalyst [28], the amount of n-butanol formed was even fifteen times higher than that of the pure support, whereas Pd as a dopant tended to produce undesired side reactions. Using the transition metals Co and Ni as dopants [29], an eight times higher reaction rate towards n-butanol was found for Co, whereby this dopant was above all active in the initial dehydrogenation step.

Finally, some additional papers report on different other factors influencing the catalytic behavior. Liang at al. also made use of CeO_2 and observed a direct correlation between reactivity and the quantity of O_2 vacancies in the catalyst bulk [30]. Bhasker-Ranganath et al. [31] used in situ DRIFTS and DFT calculations to determine that crotonaldehyde was predominantly formed when acetaldehyde flew over their ceria nanooctahedra catalyst at room temperature. Furthermore, the DFT calculations proved that the enolization of 3-hydroxybutanal revealed the highest activation barrier of the mechanistic reaction steps on the catalyst surface. Earley et al. [32] conducted a study of six Cu-based catalysts with different supports, such as Al_2O_3, TiO_2, ZSM-5, and CeO_2 with a high surface area ($HSACeO_2$) and conventional CeO_2 for the formation of butanol from ethanol. Cu on $HSACeO_2$ was found to be most promising to catalyze the dehydrogenation, condensation, and re-hydrogenation steps and to give yields of more than 30% n-butanol. Jiang et al. investigated catalysts based on Cu and CeO_2 for the reaction of ethanol into n-butanol. They obtained a yield of almost 20% butanol at a selectivity of 40%. They related these promising values to the high dispersion of Cu and CeO_2 on the activated carbon support. Using SiO_2 and Al_2O_3, respectively, instead of CeO_2 lead to higher ethyl acetate and lower n-butanol yields [33]. Furthermore, Jiang et al. employed nano-Pd catalysts for a long-term test with a yield of 24.2% [34]. In addition, Quesada et al. investigated Au nanoparticles on TiO_2 [35]. Based on their findings, the authors assigned two functions to the Au

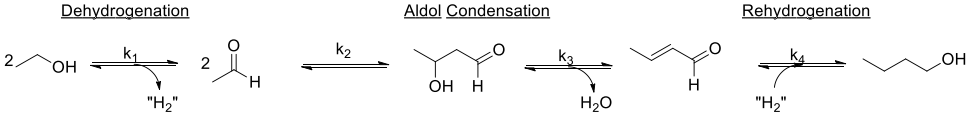

Fig. 1. Reaction scheme for the Guerbet reaction yielding n-butanol.

nanoparticles: favoring the initial dehydrogenation step of the Guerbet reaction and improving the final hydrogenation to yield n-butanol. Based on their experimental findings with zeolites doped with alkali cations, Yang and Meng proposed a substantially different mechanism compared to that shown in Fig. 1 [36]. They conclude that no acetaldehyde formation via dehydrogenation of ethanol occurs. Instead, two ethanol molecules condense by dehydration. Thereby, the C–H bond in the β-position of one of the ethanol molecules is activated via basic sites in the zeolite. A similar mechanism is postulated by Yang et al. [37].

2. Experimental

2.1. Inductively-coupled plasma combined with optical emission spectrometry (ICP-OES)

The experiments were performed with an iCAP 6500 apparatus from Thermo Fisher Scientific. For each catalyst (Dy_2O_3/C, Eu_2O_3/C and Er_2O_3/C), an aliquot of 20 mg was extracted with an aqua regia for 18 h at a temperature of 80 °C. Each catalyst solution was then filled up to a total volume of 50 mL. Two dilutions of each catalyst solution (one hundred- and ten-fold) were then produced and analyzed.

2.2. Scanning transmission electron microscopy (STEM)

The synthesized powder samples were analyzed using a probe-corrected Scanning Transmission Electron Microscopy (STEM) Hitachi HF5000 cold FEG electron microscope operated at 200 kV. The apparatus was equipped with a dark field (DF), bright field (BF), and secondary electron (SE) detector, as well as two UltiMax TLE Oxford Instruments detectors with nominal collection angles of ~1.1 srad each, so as to acquire energy-dispersive X-ray (EDX) data for chemical distribution analysis. For sample preparation, the powder samples were ground in an ethanol solution for several minutes and drop-casted onto a Cu-carbon-film grid.

2.3. N_2 sorption

The experiments with respect to the catalysts' surface areas were run using the corresponding experimental description in [38]. The Brunnauer-Emmett-Teller method was also employed [39].

2.4. Temporal analysis of products (TAP)

In the "Results and discussion" section, the specific expressions "Height-normalized response," "Ar normalized response," and "Mass corrected time" are used. These terms mean the following:

- In order to normalize the experimental outlet fluxes with respect to their heights, the single discrete values of the respective trends were divided by the maximum value of each curve. This was done to ease the comparison of the residence times of the components leaving the TAP micro-reactor.
- For the Ar-normalized response, which is used to compare trends among the single components in the reactor outlet at different temperatures, the single discrete values of the response pulses at a specific temperature are multiplied by the quotient of the maximum Ar peak at the maximum temperature to the maximum Ar peak at the specific temperature.
- The mass-corrected time is obtained when the time values of a specific component's response are multiplied by the square root of the quotient (M_{Ar}/M_{gas}). In this quotient, M_{Ar} represents the molar mass of Ar and M_{gas} that of the specific component. This arithmetic operation reflects the fact that delays or expeditions of specific molecules at the outlet of the TAP reactor compared to the residence time of the Ar (only diffusion) are also influenced by the respective molar masses.

2.4.1. Experimental procedure

Three types of TAP experiments were performed for this work:

(i) Pulsing acetaldehyde onto the surfaces of Dy_2O_3/C, Eu_2O_3/C, and Er_2O_3/C, at temperatures between 150 °C and 350 °C in the transient mode under ultra-high vacuum conditions:

The TAP micro-reactor was filled with 20 mg of the respective catalysts, which were reduced at atmospheric pressure and 250 °C in a flow of 2.5 vol% H_2/Ar for 1 h. During pulsing, the concentration of acetaldehyde amounted to 38.3 mol% in Ar. This was adjusted by, at first, evacuating the tank, then injecting liquid acetaldehyde into it, increasing the pressure therein to 23 PSI by adding Ar and finally heating it to 20 °C. Using the Antoine equation with its various constants for acetaldehyde [40], the mentioned concentration for acetaldehyde was attuned. All TAP installations (lines, manifolds with pulse valves) between the tank and micro-reactor were stoked to 40 °C to ensure that acetalydehyde could not condense in these parts.

(ii) Pulsing mixtures of CO/Ar, CH_4/Ar, H_2/Ar, butanol/Ar, and crotonaldehyde/Ar, respectively, on Dy_2O_3/C in the temperature range between 150 °C and 350 °C in transient mode under ultra-high vacuum conditions:

For all adsorption experiments, 20 mg of Dy_2O_3/C were funneled into the micro-reactor and reduced at atmospheric pressure and 250 °C in a flow of 2.5 vol% H_2/Ar for 1 h. During pulsing, the molar concentrations of CO, CH_4 and H_2, respectively, were the same and amounted to 50% in Ar. In the case of butanol adsorption, the tank containing the butanol was pressurized with Ar to a value of 25 PSI before the lines and manifold were heated to 120 °C. For crotonaldehyde adsorption, the pressure in the tank filled with crotonaldeyhde was also increased to 25 PSI using Ar and the temperatures of all of the lines and manifold were set to 110 °C. On the basis of the Antoine constants of butanol and crotonaldeyhde, molar concentrations of 38.6% and 42.7%, respectively, were set.

(iii) Injecting a series of 7000 acetaldehyde pulses onto the surface of Dy_2O_3/C at 200 °C in transient mode under ultra-high vacuum conditions:

For the long series of acetaldehyde pulsing, a pre-reduced (250 °C using He/Ar) Dy_2O_3/C catalyst was used. To set the molar acetaldehyde concentration at 29.0%, the evacuated tank was filled with acetaldehyde before the pressure was increased to 35 PSI using Ar. All lines had a temperature of 40 °C, whereas that of the tank was 20 °C.

A TAP-KPC Multi-Experiment system was used to conduct the TAP experiments between 100 °C and 350 °C. The reactor (4.8 mm i.d. and 33.9 mm length, length of the catalyst zone: 0.6 mm) was filled with 20 mg of catalyst particles (0.2–0.4 mm) and packed between two layers of quartz particles. The catalyst sample was placed in the isothermal zone of the reactor with a height of approximately 1 mm. A mass spectrometer (Stanford Research Systems RGA 200) was used to record the experimental outlet fluxes presented in the figures of this paper. The following m/z-values were selected for the respective components: 2 for H_2, 16 for CH_4, 28 for CO, 29 for acetaldehyde, 40 for Ar, 56 for butanol, 69 for crotonaldehyde, and 72 for butyraldehyde. In addition, m/z-values of 60 (acidic acid), 61 (ethyl acetate), and 59 (diethyl ether) were investigated at each temperature for all catalysts, but in any case the response pulses did not exhibit a measurable maximum.

2.5. Catalyst preparation

The oxides of the lanthanides were dissolved in HNO_3 at 160 °C. Next, the solution was diluted with deionized H_2O, yielding 2.5 mL in total. This volume was then impregnated onto 5 g of activated carbon (Merck KGaA). The precursor was calcined at 500 °C for 4 h under a flow

of N_2.

3. Results and discussion

3.1. Inductively-coupled plasma optical emission spectrometry (ICP-OES)

Table 1 presents the mean mass fractions of some relevant elements in the catalysts Dy_2O_3/C, Eu_2O_3/C, and Er_2O_3/C. In any case, the desired components Dy, Eu and Er, respectively, were found to be predominant. Only in the case of Dy_2O_3/C were some minor quantities of Fe detected. It can be concluded that the preparation process was successful for all catalysts.

3.2. Scanning transmission electron microscopy (STEM)

The morphology of the three catalysts, Dy_2O_3/C, Eu_2O_3/C, and Er_2O_3/C, and the dispersion of the co-deposited catalytic particles on the activated carbon material, were analyzed using STEM and acquiring high-angle annular dark field (HAADF) images in combination with EDX elemental mapping to identify the observed particles. The underlying principle of HAADF is that Rutherford-scattered electrons from the atomic nucleus are detected at an annular detector below the specimen. Due to this kind of scattering being dependent on the atomic number Z, heavier atoms appear with a brighter contrast than atoms with a lower Z. In this case, this allows the distinguishing of different metals from the C support, shown here for the overview images on the left-hand side in Fig. 2. The corresponding element maps of the same area are placed next to the HAADF, followed by the individual element distribution image of Dy_2O_3/C, Eu_2O_3/C, and Er_2O_3/C, respectively. Surprisingly, the EDX measurements did not only reveal the expected metals but also Si was found via the EDX measurement in the cases of Er_2O_3/C and Eu_2O_3/C, which was not observed during the ICP–OES investigation. Although Dy and Eu were fairly uniformly distributed over the surface of the activated carbon support, some agglomerations occurred in the case of Er.

3.3. N_2 sorption

Table 2 lists the specific surface areas of Dy_2O_3/C, Eu_2O_3/C, and Er_2O_3/C. It becomes obvious that they are very similar, with values of between 606 $m^2\ g^{-1}$ for Eu_2O_3/C and 632 $m^2\ g^{-1}$ for Er_2O_3/C.

3.4. TAP

The first introductory experiments in this study were performed to understand the pure adsorption and desorption behaviors of the possible reaction products of acetaldehyde pulsing on Dy_2O_3, which are not influenced by chemical reactions and their single steps and intermediates on the catalyst surface. It was derived from former experiments with respect to ethanol pulsing on Pt/C, Ir/C, and Cu/C [38] that acetaldehyde might decompose into CO, CH_4, and H_2 in addition to its aldol condensation reaction. With respect to the latter reaction, the adsorption and desorption behaviors of butanol and crotonaldehyde, respectively, were also investigated.

For the experiments depicted in Fig. 3a)–d), mixtures of 50 vol% CO, CH_4, and H_2, respectively, in Ar were pulsed onto the surface of Dy_2O_3/C at temperatures between 150 and 350 °C. Thereby, the response pulses of Ar represent the diffusion-only case without any interaction with the catalytic material. Any deviation of the trends of CO, CH_4 and H_2, respectively, from this diffusion-only case is directly linked to chemical interference with the catalyst. Fig. 3a)–c) show that the desorption of all three molecules CO, CH_4, and H_2 was independent of the temperature between 150 and 350 °C. Quantitative analyses revealed that of all the reaction temperatures, approximately 100% of the adsorbed molecules reversibly desorbed from the catalyst surface. In each case, the energy barrier for desorption could be raised. CO, CH_4, and H_2 did not strongly stick to the Dy_2O_3/C surface. In addition, Fig. 3d) depicts the order in which CO, CH_4, and H_2 desorbed from the catalyst surface at a typical temperature of 250 °C. Their height-normalized trends are outlined as a function of the mass-corrected time, complemented by that of Ar for the means of comparison. It becomes obvious that in their rising segments, the response pulses of CH_4 and CO coincided and were only slightly delayed compared to the trend for Ar. These CH_4 and CO molecules only minimally interacted with the catalyst. However, at residence times longer than approximately 0.06 s, the deviations of the CH_4 and CO curves from that of Ar became more pronounced, indicating more complex processes like adsorption and desorption on the Dy_2O_3/C surface. This development was stronger in the case of CH_4. The experimental outlet flux of H_2 in Fig. 3d) considerably differs from the other ones, as it is much broader and displays an intense tailing at longer residence times. This shape of the H_2 curve could be due to dissociative H_2 adsorption and subsequent spill-over processes of H-atoms from the Dy_2O_3 particles to the activated carbon support and vice versa. These processes are often reported for different catalysts in the literature [41–44]. It is highlighted in relevant papers that H-spillover is a beneficial property of catalysts with respect to their H_2 storage and hydrogenation activity.

In addition to the trends shown in Fig. 3, Fig. 4 displays the response pulses of butanol a) and crotonaldehyde b), respectively, when these substances were pulsed onto Dy_2O_3/C at temperatures of between 150 and 350 °C. In the case of butanol pulsing in Fig. 4a) on the left, a clear influence of the temperature was observed. Butanol desorption was strongest at 200 and 250 °C and then became weaker at 300 and 350 °C. Quantitative analyses indicated low values for the percentage of reversibly-desorbing butanol molecules of approximately 16% at 200 and 250 °C and only roughly 8% at 300 and 350 °C. In contrast to CO, CH_4, and H_2, most butanol molecules strongly stuck to the Dy_2O_3/C surface in the investigated temperature range. In the case of crotonaldehyde (see Fig. 4b)), the situation is slightly different. The intensity of desorption is very low at temperatures between 150 and 250 °C and becomes significantly higher at 300 and 350 °C. Quantitative analyses, however, proved that only 10% of the adsorbed crotonaldehyde molecules desorbed again from the catalyst surface at 350 °C. At lower temperatures, these values were in the range of less than 5%. Across the entire temperature range, most crotonaldehyde molecules strongly stuck to the surface of Dy_2O_3/C, even more so than the butanol molecules did. Consequently, the desorption trends exhibited a very broad tailing. Similar adsorption and desorption behaviors were observed in the cases of the catalysts Eu_2O_3/C and Er_2O_3/C.

The next figure confirms the assumption from Fig. 3 concerning the possible formation of CO, CH_4, and H_2. It depicts the residence time distribution of all relevant substances in the outlet of the TAP microreactor at a typical reaction temperature of 250 °C after acetaldehyde pulsing (38.3 vol% in Ar) on the catalytic surface of Dy_2O_3/C. It becomes clear that not only were the desired products of crotonaldehyde and butanol formed but also those of acetaldehyde decomposition, CO, CH_4, and H_2. The formation of CO was very rapid and CO desorbed

Table 1
Averaged mass fractions of relevant elements in the three investigated catalysts supported on activated carbon.

Element	Unit	Dy_2O_3/C	Eu_2O_3/C	Er_2O_3/C
Ni	ma%	< 0.01	< 0.008	< 0.005
Si	ma%	< 0.01	< 0.01	< 0.006
Pd	ma%	< 0.003	< 0.002	< 0.001
Dy	ma%	7.60	< 0.008	< 0.024
Eu	ma%	< 0.003	5.61	< 0.001
Er	ma%	< 0.01	< 0.01	7.27
Ti	ma%	< 0.001	< 0.0008	< 0.0005
Cr	ma%	< 0.004	< 0.003	< 0.002
Al	ma%	< 0.07	< 0.05	< 0.03
Zn	ma%	< 0.0007	< 0.0005	< 0.0003
Fe	ma%	0.0132	< 0.003	< 0.002

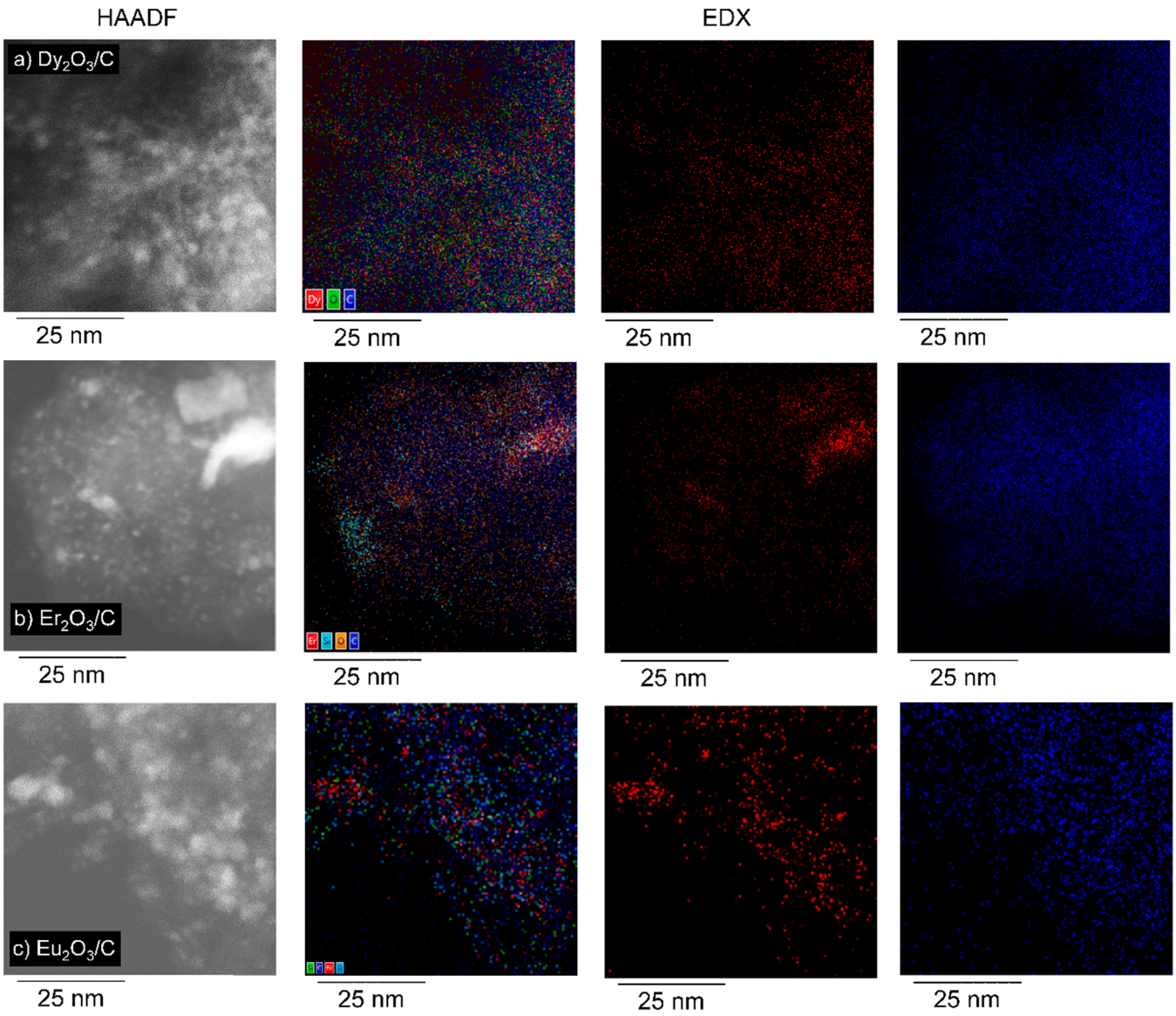

Fig. 2. HAADF–STEM images (left) with the corresponding EDX element mappings showing the combined EDX elemental map images (second from left), as well as the respective single images for the metal (red) and carbon (blue) for: a) Dy_2O_3/C; b) Er_2O_3/C; and c) Eu_2O_3/C samples. Additionally, Si is depicted in the EDX maps of the last two samples.

Table 2
Specific surface areas of Dy_2O_3/C, Eu_2O_3/C, and Er_2O_3/C.

Catalyst	Specific surface area [$m^2\ g^{-1}$]
Dy_2O_3/C	624
Eu_2O_3/C	606
Er_2O_3/C	632

quickly from the catalyst with only little interaction with the surface. However, in the cases of CH_4 and, moreover, H_2, the response pulses were strongly delayed in comparison to that of Ar (and CO), pointing to extensive reversible chemical interactions like adsorption and desorption on the catalyst surface. The residual unreacted acetaldehyde molecules desorbed on a shorter time scale than CH_4 and H_2 but plainly exhibited more interaction with the catalyst surface than CO did. At shorter residence times of up to approximately 0.5 s, crotonaldehyde and butanol desorbed on a time scale comparable to that of CO, but showed a broader tailing at longer residence times and then became congruent to that of acetaldehyde. Butanol was very quickly formed from crotonaldehyde; however, the intensities of the butanol and crotonaldehyde responses were much smaller than those of CO, CH_4, and H_2. This stands in good agreement with the findings from Fig. 4, which showed low quantities of butanol and crotonaldehyde molecules desorbing from the surface of Dy_2O_3/C at 250 °C. Very similar residence time distributions were observed in the cases of the catalysts Eu_2O_3/C and Er_2O_3/C.

The next figures compare the delay (compared to the Ar diffusion-only case) of the CO, CH_4, and H_2 experimental outlet fluxes from Fig. 3, when the molecules were simply pulsed onto the surface of Dy_2O_3/C without a chemical reaction with those trends, when CO, CH_4 and H_2 were formed during acetaldehyde pulsing on Dy_2O_3/C. The typical reaction temperature is 350 °C. It becomes obvious that in any case, the signals from acetaldehyde pulsing were significantly broader than those from pulsing the pure single components onto the surface of Dy_2O_3/C. This effect was smallest in the case of CO and grew much more pronounced for CH_4 and especially H_2. These findings account for the rapid formation of CO from acetaldehyde, although this process requires numerous paces on Dy_2O_3/C, such as C–H and C–C bond fractures.

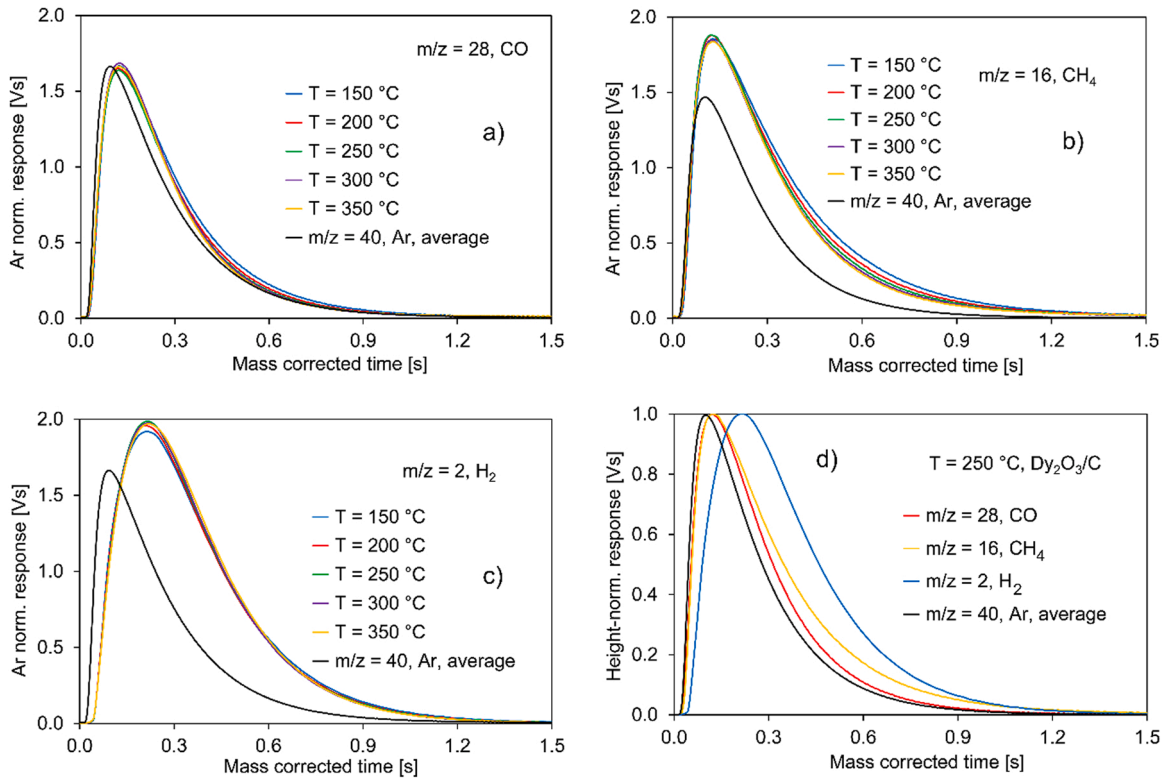

Fig. 3. a)–c) Experimental outlet fluxes (normalized to the respective Ar response pulses) when the following gas mixtures were pulsed onto the surface of Dy_2O_3/C at temperatures between 150 °C and 350 °C: a) 50 vol% CO in Ar; b) 50 vol% CH_4 in Ar; and c) 50 vol% H_2 in Ar. d) Response pulses (normalized to the respective maximum peak heights) of CO, CH_4, and H_2 at 250 °C when the same gas mixtures from Fig. 3a)–c) were pulsed onto Dy_2O_3/C, averaged Ar trend for the means of comparison.

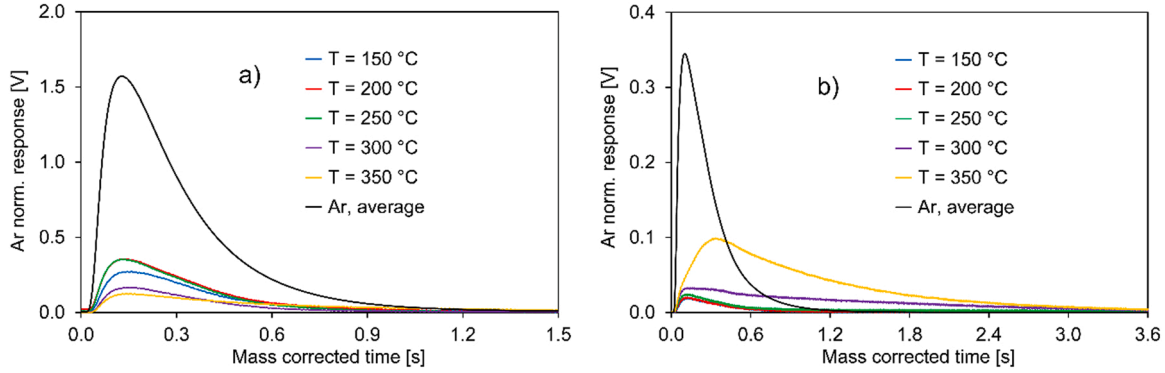

Fig. 4. a)–b) Experimental outlet fluxes (normalized to the respective Ar response pulses) of butanol (left) and crotonaldehyde (right) when the following gas mixtures were pulsed onto the surface of Dy_2O_3/C at temperatures between 150 and 350 °C: a) 38.6 vol% butanol in Ar. b) 42.7 vol% crotonaldehyde in Ar.

Clearly – and this explains the distinct tailings of the CH_4 and H_2 trends – the formation of CH_4 and, moreover, H_2 is governed by rather slow steps on Dy_2O_3/C, such as the above-mentioned H-spillover and, additionally, CH_3 spillover [45]. (Figs. 5 and 6).

Fig. 7 depicts the experimental outlet fluxes of acetaldehyde at different reaction temperatures of between 100 and 350 °C after acetaldehyde pulsing (38.3 vol% in Ar) onto the catalytic surface of Dy_2O_3/C. The figure shows that at a temperature of 100 °C, only a fairly small response pulse with a maximum at a residence time of approximately 0.2 s was observed. At this temperature, most acetaldehyde molecules were irreversibly adsorbed onto the catalyst surface and the calculated acetaldehyde conversion was 96%. At 150 °C, the acetaldehyde transient is more complex and shows an initial, rather small peak at low residence times, which is almost congruent with the Ar-curve, indicating that a small number of acetaldehyde molecules only very weakly interacted with the catalyst surface. However, at residence times longer than 0.09 s, the response pulse for acetaldehyde became very broad, hinting at extensive reversible chemical interactions with the catalyst surface. Due to the increased temperature, plainly more molecules desorbed from the catalyst surface compared to the curve at 100 °C. The conversion of acetaldehyde amounted to 67%. While further increasing the reaction temperature to 200 °C, 250 °C, and 300 °C, respectively, the acetaldehyde transients became significantly narrower and higher. The extent to which the acetaldehyde molecules interacted with the catalyst surface decreased between 200 and 300 °C, and at the same time the acetaldehyde conversion increased from 16% at 200 °C to 45% at 250 °C, and 58% at 300 °C. At 350 °C, the transient response for acetaldehyde became even smaller and narrower than at 300 °C and the

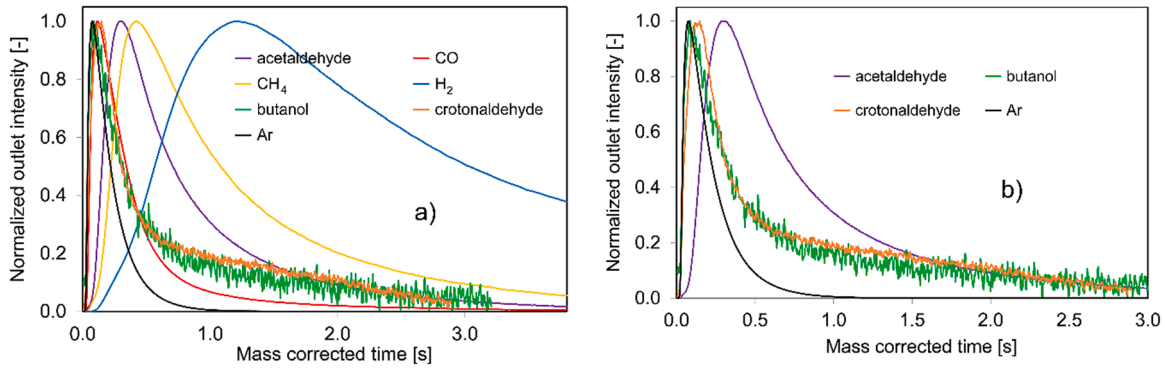

Fig. 5. Experimental outlet fluxes (normalized to the height) when acetaldehyde (38.3 vol% in Ar) was pulsed on Dy_2O_3/C at 250 °C belonging to different components as indicated in the figure.

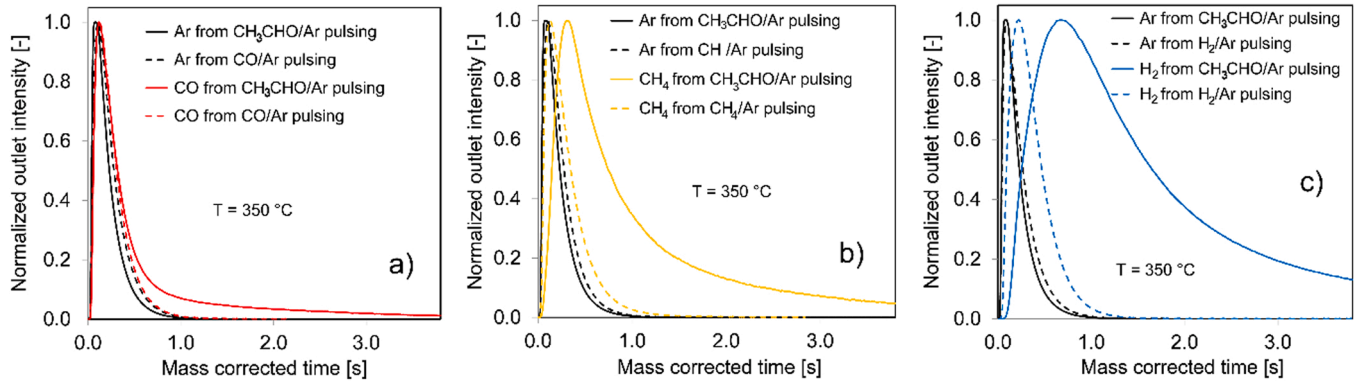

Fig. 6. Comparative analysis of the experimental outlet fluxes (normalized to the height) of CO, CH_4, and H_2 when: (i) acetaldehyde (38.3 vol% in Ar) was pulsed on Dy_2O_3/C; and (ii) pure gas mixtures of 50% CO/Ar, 50% CH_4/Ar, and 50% H_2/Ar, respectively, were pulsed on Dy_2O_3/C, all corresponding Ar trends for the means of comparison, T = 350 °C.

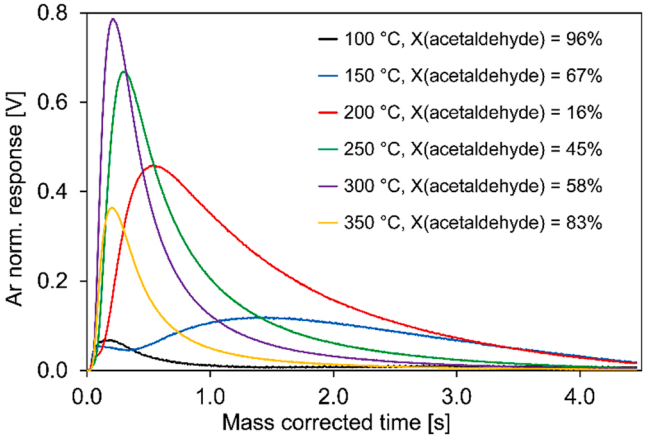

Fig. 7. Experimental outlet fluxes (normalized to the respective Ar transients) at an *m/z*-value of 29 for acetaldehyde when acetaldehyde (38.3 vol% in Ar) was pulsed on Dy_2O_3/C at temperatures between 100 and 350 °C.

acetaldehyde conversion reached a value of 83%. The trend of the acetaldehyde conversion between 200 and 350 °C makes it clear that the desorption of acetaldehyde from the catalyst surface or its further reaction was favored by the higher enthalpy flow. Reaction Eq. (1) reflects the trends depicted in Fig. 7:

$$2\ CH_3CHO \leftrightarrow CH_3CHO + CH_3CHO^* \quad (1)$$

The following mathematical Eqs. (2)–(6) explain how activation energy estimates for the desorption of acetaldehyde from the catalyst surfaces or its further reaction were calculated. When pulsing an inert molecule, such as Ar, over inert material (quartz in this case), the experimentally determined mean residence time of Ar $\tau_{Ar,in}$ can be related to the Ar diffusivity $D_{Ar,in}$ according to Eqs. (1) and (2).

$$\tau_{Ar,in} = \frac{M_1}{M_0} \quad (2)$$

$$D_{Ar,in} = \frac{\varepsilon * L^2_{reactor} *}{\tau_{Ar,in} * 2} \quad (3)$$

In these equations, M_0 and M_1 are the zeroth and first moments of the Ar response pulse over inert material, ε is the void fraction of the inert material (0.45 in this case) and $L_{reactor}$ is the total reactor length (33.9 mm). From Eq. (2), the diffusivity of acetaldehyde $D_{acetaldehyde,in}$ in the inert material can be calculated via Eq. (3). Here, M_{Ar} and $M_{acetaldehyde}$ are the molar masses of Ar and acetaldehyde, respectively. T is the temperature at which the diffusivity is needed and T_{Ar} is the temperature at which the diffusivity of Ar in the inert material was measured.

$$D_{acetaldehyde,in} = D_{Ar,in} * \sqrt{\frac{M_{Ar}}{M_{acetaldehyde}}} * \sqrt{\frac{T}{T_{Ar}}} \quad (4)$$

In general, the diffusivity in the inert zones of the TAP micro-reactor is not the same as the diffusivity in the catalyst zone, unless a completely non-porous catalyst is used. However, taking into account that the catalyst zone is very thin (0.6 mm) in relation to the total length of the reactor (33.9 mm) it can be approximated that the divergent diffusivity in the catalyst zone does not affect the response pulses of inert gases and

reactants, respectively, very much. To calculate the residence time of actetaldehyde $\tau_{acetaldehyde,cat}$ inside the catalyst zone, Eq. (4) can be applied, which considers only the diffusivity of acetaldehyde $D_{acetaldehyde,in}$ in the inert material, as the molecules spend most of their time in this section of the reactor.

$$\tau_{acetaldehyde,cat} = \frac{L_{cat} * L_{in}}{D_{acetaldehyde,in} * 2} \quad (5)$$

In this equation, L_{cat} and L_{in} are the length of the catalyst zone and the total length of the two inert zones above and below the catalyst, respectively. Now, the apparent reaction constants k_{app} at specific reaction temperatures can be calculated according to Eq. (5) taking into account the conversion X of acetaldehyde.

$$k_{app} = \frac{X_{acetaldehyde}}{\left(1 - X_{acetaldehyde}\right) * \tau_{acetaldehyde,cat}} \quad (6)$$

In this respect, Table 3 shows the calculated apparent reaction constants at reaction temperatures between 200 °C and 350 °C for the three different catalysts Dy_2O_3/C, Eu_2O_3/C, and Er_2O_3/C. Based on these data, Arrhenius plots provide estimates for the activation energies of the desorption or further reaction of acetaldehyde. These are 52 kJ mol^{-1} for Dy_2O_3/C, 66 kJ mol^{-1} for Eu_2O_3/C, and 58 kJ mol^{-1} for Er_2O_3/C, respectively.

The next figure illustrates the extent to which the other reaction products from Fig. 5 (CO, CH_4, H_2, crotonaldehyde, butanol) desorbed from the surface of Dy_2O_3/C at different reaction temperatures. In Fig. 8a), it can be seen that the height of the experimental outlet fluxes of CO slightly increased with rising reaction temperatures. All six trends coincided in their rising sections. However, they became broader and with a more profound tailing when the temperature increased. This indicates more complex interactions between the CO molecules and catalytic sites.

$$S = \frac{\left(n_k - n_{k,0}\right) * \upsilon_{acetaldehydei}}{\left(n_{acetaldehyde,0} - n_{acetaldehyde}\right) * \upsilon_k} \quad (7)$$

When analyzing the molar outlet amount of CO as shown in Table 4, almost constant values in the temperature range between 200 and 350 °C were observed. The calculations of the selectivities towards CO in this table according to Eq. (7) show a high value of 42.2% at 200 °C when the acetaldehyde conversion was only 16%. In equation (7), n_k is the molar outlet amount of a specific component k and $n_{k,0}$ its corresponding inlet amount. Furthermore, $n_{acetaldehyde,0}$ is the molar inlet amount of acetaldehyde and $n_{acetaldehyde}$ the outlet amount at different temperatures. The stoichiometric factors are represented by υ_k and $\upsilon_{acetaldehyde}$. At higher temperatures, however, the selectivities towards CO strongly decreased to values of 13.2%, 11.2%, and 8.7%, respectively. The values for the molar outlet amount of CO and the respective selectivities do not explain the increasing trend of the acetaldehyde conversion observed in Fig. 7 between 200 and 350 °C. A considerably different picture emerges in the case of the time- and temperature-dependent desorption of CH_4 from the surface of Dy_2O_3/C in Fig. 8b). At 100 °C, only a very small desorption peak was observed, which means that CH_4 was formed at low quantities or that it strongly stuck to the catalyst surface. At 150 °C, initially a small peak at a residence time of 0.2 s was found, followed by a very broad tailing that hinted at slow processes governing the CH_4 desorption from the surface of Dy_2O_3/C. As in the case of acetaldehyde desorption, the CH_4 trends became more narrow and higher when the reaction temperature was in the range between 200 and 300 °C. When looking at the molar outlet amounts of CH_4 between 200 and 300 °C in Table 4, it becomes obvious that they were inversely proportional to the conversions of acetaldehyde. It was highest at 200 °C when the acetaldehyde conversion was only 16% and continuously decreased while in parallel the acetaldehyde conversion increased to 58% at 300 °C. This inverse trend continued at 350 °C, when the CH_4 molar outlet amount further decreased while the acetaldehyde conversion reached its maximum value of 83%. In addition, as in the case of CO, a considerably decreasing trend of the selectivities towards CH_4 from 48.1% to 3.6% was observed between 200 and 350 °C. These findings mean that additional components in the product spectrum other than CO and CH_4 or species strongly sticking to the surface must be responsible for the increasing trend of the acetaldehyde conversion between 200 and 350 °C. In this respect, Fig. 8c) shows the time- and temperature-dependent experimental outlet fluxes of H_2 when acetaldehyde was pulsed on Dy_2O_3/C. It can be seen that H_2 desorption at 100 and 150 °C was negligible in comparison to the large quantities of desorbing H_2 molecules at 300 °C and, especially, 350 °C. In parallel, the molar outlet amount and selectivity towards H_2 with a value of almost 30% were by far highest at 350 °C (see Table 4). However, when summing up the selectivities towards CO, CH_4, and H_2 at, e.g., 350 °C, it is clear that other components, which strongly stick to the catalyst surface, such as crotonaldehyde or butanol, or adsorbates on the catalyst surface, such as CH_3 groups or carbonaceous deposits, must be of importance.

In this respect, the experiment shown in Fig. 9 deals with the question of whether acetaldehyde pulsing leads to coke formation on Dy_2O_3/C. It compares the response pulses of CO and CO_2 to pulses of 50 vol% O_2 in Ar prior to and after 7000 pulses of acetaldehyde onto the surface of Dy_2O_3/C at 200 °C. It is evident in Fig. 9 that both trends revealed a much higher intensity as a result of the series of acetaldehyde pulses. This is clear evidence that carbonaceous deposits play an important role at the catalyst sites. In addition, Fig. 9c) shows which way the O_2 response pulses evolved during O_2 pulsing onto Dy_2O_3/C at 200 °C. The first experimental outlet fluxes had very low intensities, indicating almost complete consumption of O_2 via the reactions with the coke deposits. As the number of O_2 pulses increased, the intensities of the O_2 trends became continuously larger, which means that the extent to which the surface of Dy_2O_3/C was covered by carbonaceous deposits decreased. It can be assumed that the catalyst surface can be regenerated to considerable extents.

Reaction Eqs. (8)–(10) reflect the findings from the previous figures and Table 4 with respect to the formation of CO, CH_4, H_2 and carbonaceous deposits on the surface of Dy_2O_3/C. The spillover processes in reactions (9) and (10) explain the large delays and profound tailings of the response pulses of H_2 and CH_4. Reaction (10) was strongly favored by higher reaction temperatures, leading to the large quantities of desorbing H_2 observed in Fig. 8c), which in turn – jointly with coke formation, irreversibly sticking methyl groups and strongly adsorbing butanol and crotonaldehyde molecules – explains the increasing conversion of acetaldehyde shown in Fig. 7. As a result, the quantity of available adsorbed H-species on the catalyst surface decreased to some extent when the reaction temperature rose, which discriminated the reaction rate of step (9) and led to the declining trend of the molar outlet amount of CH_4 and its selectivities in Table 4 between 200 and 350 °C.

$$2\ CH_3CHO^* \leftrightarrow 2\ CO + C^* + CH_3^* + 5\ H^* \quad (8)$$

$$CH_3^* + H^* \rightarrow \text{spillover} \rightarrow CH_4 \quad (9)$$

$$H^* + H^* \rightarrow \text{spillover} \rightarrow H_2 \quad (10)$$

As a complement to Fig. 8a)–c), Fig. 8d) and e) present the time- and temperature-dependent experimental outlet fluxes of crotonaldehyde

Table 3
Apparent reaction constants for the desorption or further reaction of acetaldehyde on Dy_2O_3/C, Eu_2O_3/C, and Er_2O_3/C at temperatures between 200 °C and 350 °C.

Temperature [°C]	k_{app} (Dy_2O_3/C) [s^{-1}]	k_{app} (Eu_2O_3/C) [s^{-1}]	k_{app} (Er_2O_3/C) [s^{-1}]
200	11.5	13.3	6.7
250	52.1	50.0	32.8
300	92.1	171.4	95.9
350	339.4	799.4	246.5

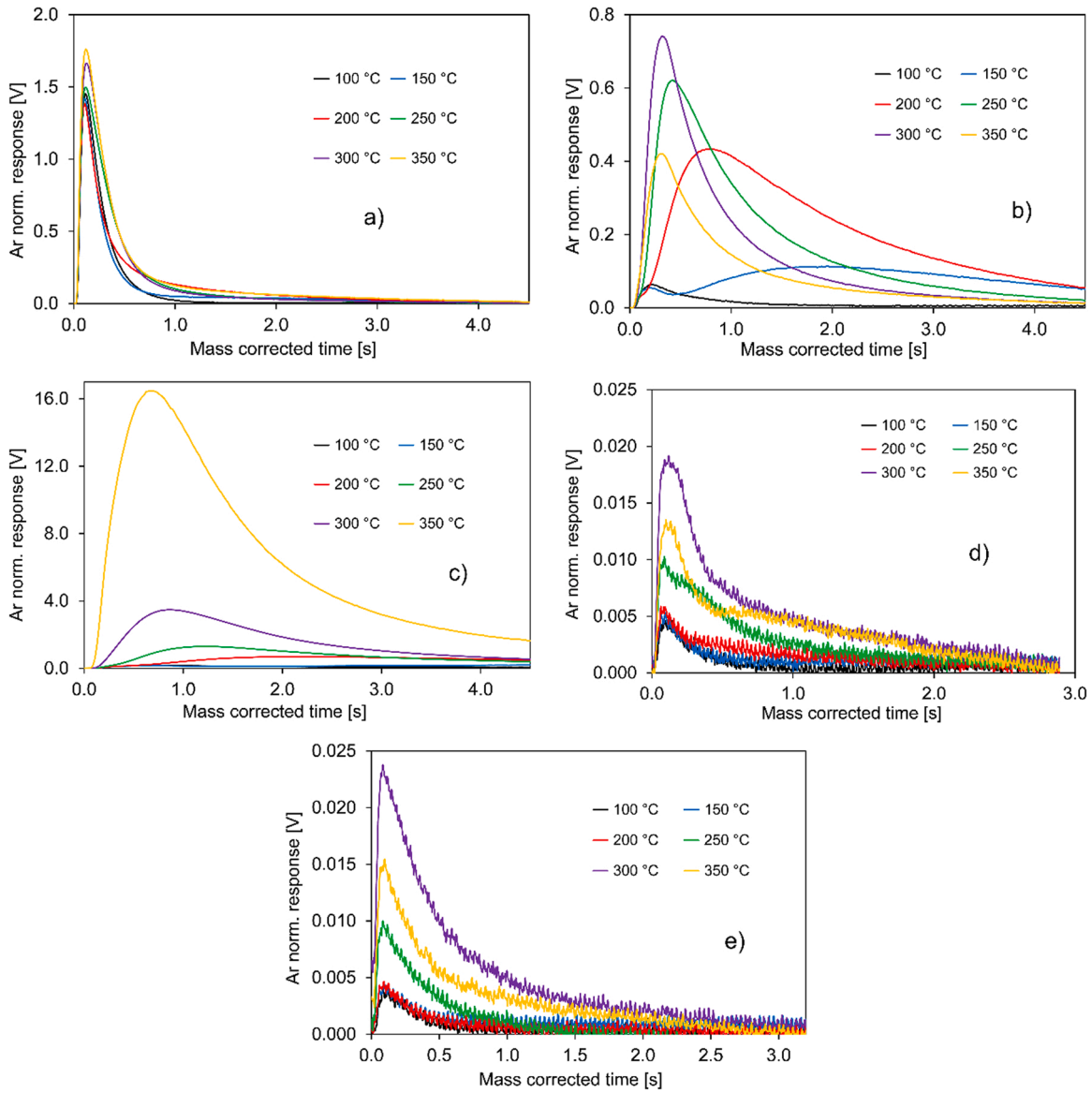

Fig. 8. Experimental outlet fluxes (normalized to the respective Ar transients) when acetaldehyde (38.3 vol% in Ar) was pulsed on Dy_2O_3/C at temperatures between 100 and 350 °C at an *m*/*z*-value of: a) 28 for CO, b) 16 for CH_4, c) 2 for H_2, d) 69 for crotonaldehyde, e) 56 for butanol.

Table 4
Molar outlet amounts and selectivities towards CO, CH_4, and H_2 as a function of the temperature when acetaldehyde (38.3 vol% in Ar) was pulsed on Dy_2O_3/C.

Temperature [°C]	Molar outlet amount CO [mole]	S (CO) [%]	Molar outlet amount CH_4 [mole]	S (CH_4) [%]	Molar outlet amount H_2 [mole]	S (H_2) [%]
100	$1.28 * 10^{-9}$	2.1	$0.11 * 10^{-9}$	0.3	$0.06 * 10^{-9}$	0.1
150	$1.52 * 10^{-9}$	6.4	$0.80 * 10^{-9}$	3.4	$0.36 * 10^{-9}$	1.5
200	$2.04 * 10^{-9}$	42.2	$2.32 * 10^{-9}$	48.1	$1.04 * 10^{-9}$	21.6
250	$1.96 * 10^{-9}$	13.2	$1.73 * 10^{-9}$	11.7	$1.02 * 10^{-9}$	6.9
300	$2.02 * 10^{-9}$	11.2	$1.45 * 10^{-9}$	8.0	$1.97 * 10^{-9}$	10.9
350	$2.18 * 10^{-9}$	8.7	$0.90 * 10^{-9}$	3.6	$7.48 * 10^{-9}$	29.7

and butanol when acetaldehyde was pulsed on Dy_2O_3/C. For both molecules, the intensities of the response pulses were rather low in comparison to those of CO, CH_4, and H_2, but slightly enhanced with increasing temperature. This confirms the findings from Fig. 4 and Fig. 5 that, in addition to acetaldehyde decomposition, the desired homo aldol condensation takes place on the catalyst surface of Dy_2O_3/C and that the quantities of desorbing butanol and crotonaldehyde molecules are low under the TAP reaction conditions. Reaction Eqs. (11) and (12) consider

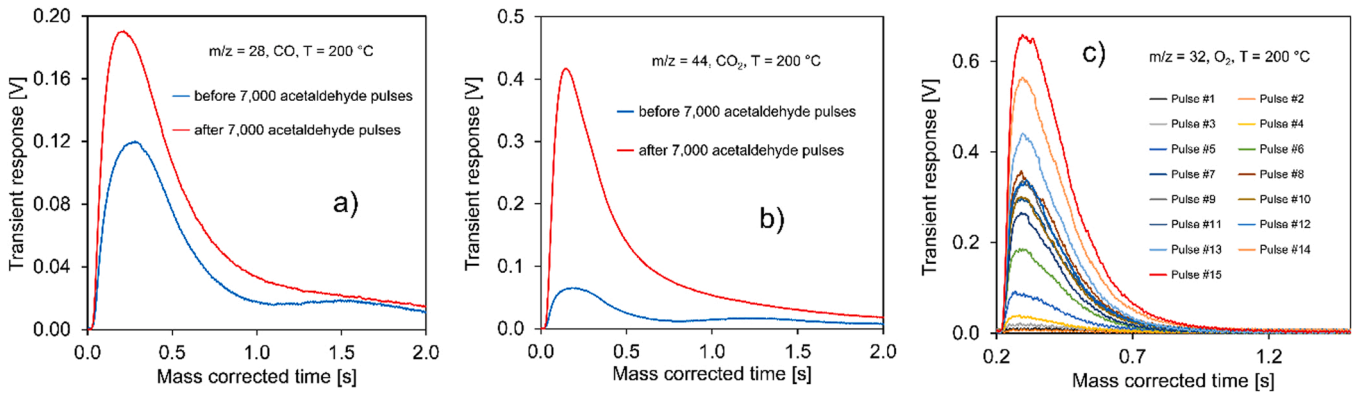

Fig. 9. Experimental outlet fluxes of CO (a), CO_2 (b), and O_2 (c), when O_2 (50 vol% in Ar) was pulsed onto the surface of Dy_2O_3/C prior to and after 7000 pulses of acetaldehyde (38.3 vol% in Ar) at 200 °C.

the formation of crotonaldehyde and then – following hydrogenation – butanol:

$$2\ CH_3 - CHO^* \leftrightarrow CH_3 - CH = CH - CHO + H_2O \quad (11)$$

$$CH_3 - CH = CH - CHO + 2\ H_2 \leftrightarrow CH_3 - CH_2 - CH_2 - CH_2OH \quad (12)$$

Fig. 10 compares the experimental outlet fluxes of crotonaldehyde and butanol, respectively, for the different catalysts Dy_2O_3/C, Eu_2O_3/C, and Er_2O_3/C to pulses of acetaldehyde. The typical reaction temperatures were 250 and 300 °C. For both, the reaction intermediate crotonaldehyde and the final product butanol, the intensities of the trends yielded with the Eu_2O_3/C catalyst were the highest at both investigated temperatures. Eu_2O_3/C is the catalyst with the highest basicity and the least pronounced balance between basic and acidic sites among the investigated samples. In this way, the findings from this figure give an answer to the research interrogation of the paper whether strong basic properties or a balanced ratio between basic and acidic sites are more beneficial for the aldol condensation within the Guerbet reaction.

4. Conclusions

By applying the TAP methodology under ultra-high vacuum conditions, it was found that the homo aldol condensation of two moles of acetaldehyde on the lanthanide oxide-based catalysts Dy_2O_3/C, Eu_2O_3/C, and Er_2O_3/C is a fairly complex process. Aside from the desired production of butanol from crotonaldehyde, acetaldehyde decomposition into CO, CH_4, H_2 and carbonaceous deposits on the catalyst surface also occurred. The desorption trends for CH_4 and H_2 were found to be very broad and strongly delayed in comparison to the diffusion-only case, indicating complex processes like H- and CH_3-spillover from the Dy_2O_3 particles to the activated carbon support and vice versa. In particular, huge amounts of H_2 desorbed from the catalyst surface at elevated temperatures of 300 and 350 °C. Adsorption/desorption experiments by pure butanol and crotonaldehyde pulsing on the surface of Dy_2O_3/C revealed that both molecules strongly stuck to the surface between 150 and 350 °C. Their desorption was only slightly favored by

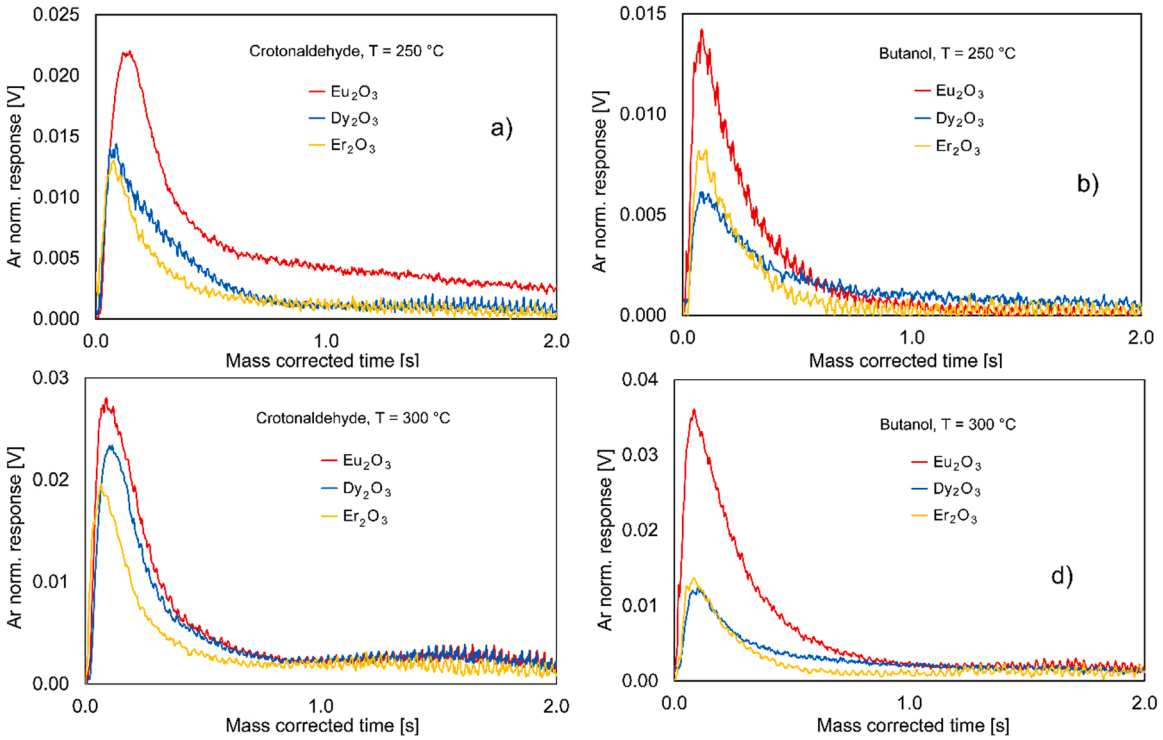

Fig. 10. Comparison of the response pulses (normalized to the Ar transients) of crotonaldehyde and butanol, respectively, to acetaldehyde (38.3 vol% in Ar) pulsing onto Dy_2O_3/C, Eu_2O_3/C and Er_2O_3/C: a) Crotonaldehyde at 250 °C, b) Butanol at 250 °C, c) Crotonaldehyde at 300 °C, d) Butanol at 300 °C.

increasing temperatures. This means that the TAP experiments cannot determine whether acetaldehyde decomposition into CO, CH_4, and H_2 or the homo aldol condensation of acetaldehyde yielding butanol is the predominant process on the catalyst surface. Carbonaceous deposits constitute a remarkable risk for catalyst deactivation by blocking catalytically-active sites. However, it was shown that they can be burnt-off again by a cascade of O_2 pulses onto the catalyst surface. Catalyst characterization demonstrated an even distribution of catalyst particles on the activated carbon support in the case of Dy and Eu and some agglomerates for Er. A large specific surface area in the range of 600 m^2/g was also found via N_2 sorption. Furthermore, by means of ICP–OES it was observed that the chosen impregnation method for catalyst preparation was successful.

CRediT authorship contribution statement

Conceptualization, **Joachim Pasel and Johannes Häusler**; Funding acquisition, **Joachim Mayer and Ralf Peters**; Investigation, **Joachim Pasel, Dirk Schmitt, Helen Valencia**; Methodology, **Joachim Pasel**; Supervision, **Joachim Mayer and Ralf Peters**; Writing – original draft, **Joachim Pasel, Helen Valencia**; Writing – review & editing, **Joachim Pasel, Johannes Häusler, Helen Valencia**.

Declaration of Competing Interest

The authors declare that they have no known competing financial interests or personal relationships that could have appeared to influence the work reported in this paper.

Data availability

Data will be made available on request.

Acknowledgements

Special thanks are due to the fuel synthesis team at Jülich and all project and cooperation partners. This study was funded by the Deutsche Forschungsgemeinschaft (DFG, German Research Foundation) – 491111487. Part of the work was funded by the project Meet HiEnd III (BMBF, Federal Ministry of Education and Research, 03XP0272C).

References

[1] N.N. Norman, A. Earnshaw, Chemistry of the Elements, 2nd ed., 1997.
[2] Z. Wang, J. Pang, L. Song, X. Li, Q. Yuan, X. Li, S. Liu, M. Zheng, Conversion of Ethanol to n-Butanol over NiCeO2 Based Catalysts: Effects of Metal Dispersion and NiCe Interactions, Ind. Eng. Chem. Res. 59 (2020) 22057–22067.
[3] S. Cimino, L. Lisi, S. Romanucci, Catalysts for conversion of ethanol to butanol: effect of acid-base and redox properties, Catal. Today 304 (2018) 58–63.
[4] H. Wang, G. Miao, L. Kong, H. Luo, Y. Zhang, X. Zhao, S. Li, Y. Sun, Efficient one-pot valorization of ethanol to 1-butanol over an earth-abundant Ni-MgO catalyst under mild conditions, Sustain. Energy Fuels 4 (2020) 1612–1615.
[5] A.S. Ndou, N. Plint, N.J. Coville, Dimerisation of ethanol to butanol over solid-base catalysts, Appl. Catal. A: Gen. 251 (2003) 337–345.
[6] M. León, E. Díaz, S. Ordóñez, Ethanol catalytic condensation over Mg-Al mixed oxides derived from hydrotalcites, Catal. Today 164 (2011) 436–442.
[7] M. León, E. Díaz, A. Vega, S. Ordóñez, A. Auroux, Consequences of the iron-aluminium exchange on the performance of hydrotalcite-derived mixed oxides for ethanol condensation, Appl. Catal. B: Environ. 102 (2011) 590–599.
[8] J. Pang, M. Zheng, L. He, L. Li, X. Pan, A. Wang, X. Wang, T. Zhang, Upgrading ethanol to n-butanol over highly dispersed Ni–MgAlO catalysts, J. Catal. 344 (2016) 184–193.
[9] K.K. Ramasamy, M. Gray, H. Job, C. Smith, Y. Wang, Tunable catalytic properties of bi-functional mixed oxides in ethanol conversion to high value compounds, Catal. Today 269 (2016) 82–87.
[10] J. Zhang, K. Shi, Z. An, Y. Zhu, X. Shu, H. Song, X. Xiang, J. He, Acid-base promoted dehydrogenation coupling of ethanol on supported Ag particles, Ind. Eng. Chem. Res. 59 (2020) 3342–3350.
[11] J. Zhang, K. Shi, Y. Zhu, Z. An, W. Wang, X. Ma, X. Shu, H. Song, X. Xiang, J. He, Interfacial sites in Ag supported layered double oxide for dehydrogenation coupling of ethanol to n-butanol, ChemistryOpen 10 (2021) 1095–1103.
[12] I.S. Pieta, A. Michalik, E. Kraleva, D. Mrdenovic, A. Sek, E. Wahaczyk, A. Lewalska-Graczyk, M. Krysa, A. Sroka-Bartnicka, P. Pieta, R. Nowakowski, A. Lew, E. M. Serwicka, Bio-dee synthesis and dehydrogenation coupling of bio-ethanol to bio-butanol over multicomponent mixed metal oxide catalysts, Catalysts 11 (2021).
[13] S. Ogo, A. Onda, Y. Iwasa, K. Hara, A. Fukuoka, K. Yanagisawa, 1-Butanol synthesis from ethanol over strontium phosphate hydroxyapatite catalysts with various Sr/P ratios, J. Catal. 296 (2012) 24–30.
[14] S. Ogo, A. Onda, K. Yanagisawa, Selective synthesis of 1-butanol from ethanol over strontium phosphate hydroxyapatite catalysts, Appl. Catal. A: Gen. 402 (2011) 188–195.
[15] D. Wang, Z. Liu, Q. Liu, Efficient conversion of ethanol to 1-butanol and C5-C9 alcohols over calcium carbide, RSC Adv. 9 (2019) 18941–18948.
[16] D. Wang, Z. Liu, Q. Liu, Synthesis of 1-Butanol from ethanol over calcium ethoxide: experimental and density functional theory simulation, J. Phys. Chem. C. 123 (2019) 22932–22940.
[17] S.C. Wang, M.C. Cendejas, I. Hermans, Insights into ethanol coupling over hydroxyapatite using modulation excitation operando infrared spectroscopy, ChemCatChem 12 (2020) 4167–4175.
[18] M. Pinzón, M. Cortés-Reyes, C. Herrera, M.Á. Larrubia, L.J. Alemany, Ca-based bifunctional acid-basic model-catalysts for n-butanol production from ethanol condensation, Biofuels, Bioprod. Bioref. 15 (2021) 218–230.
[19] G. Onyestyák, Carbon supported alkaline catalysts for guerbet coupling of bioethanol, Period. Polytech. Chem. Eng. 62 (2018) 91–96.
[20] O.M. Perrone, M.R. Siqueira, G. Metzker, D.C. de Oliveira Lisboa, M. Boscolo, Copper and lanthanum mixed oxides as catalysts for ethanol Guerbet coupling: The role of La3+ on the production of long-chain alcohols, Environ. Prog. Sustain. Energy 40 (2021).
[21] N.V. Vlasenko, P.I. Kyriienko, K.V. Valihura, G.R. Kosmambetova, S.O. Soloviev, P. E. Strizhak, Yttria-stabilized zirconia as a high-performance catalyst for ethanol to n-butanol guerbet coupling, ACS Omega 4 (2019) 21469–21476.
[22] C. Lopez-Olmos, M.V. Morales, A. Guerrero-Ruiz, I. Rodríguez-Ramos, Continuous catalytic condensation of ethanol into 1-butanol: the role of metallic oxides (M = MgO, BaO, ZnO, and MnO) in Cu-M/Graphite catalysts, Ind. Eng. Chem. Res. 59 (2020) 16626–16636.
[23] J.I. Di, Cosimo, Apesteguı, C.R.·a, M.J.L. Ginés, E. Iglesia, Structural requirements and reaction pathways in condensation reactions of alcohols on MgyAlOx catalysts, J. Catal. 190 (2000) 261–275.
[24] J.I. Di Cosimo, V.K. Díez, M. Xu, E. Iglesia, C.R. Apesteguía, Structure and surface and catalytic properties of Mg-Al basic oxides, J. Catal. 178 (1998) 499–510.
[25] J. Dai, H. Zhang, Recent advances in selective C-C bond coupling for ethanol upgrading over balanced Lewis acid-base catalysts, Sci. China Mater. 62 (2019) 1642–1654.
[26] M.B. Osman, J.M. Krafft, C. Thomas, T. Yoshioka, J. Kubo, G. Costentin, Importance of the nature of the active acid/base pairs of hydroxyapatite involved in the catalytic transformation of ethanol to n-butanol revealed by operando DRIFTS, ChemCatChem 11 (2019) 1765–1778.
[27] J. Quesada, L. Faba, E. Díaz, S. Ordóñez, Copper-basic sites synergic effect on the ethanol dehydrogenation and condensation reactions, ChemCatChem 10 (2018) 3583–3592.
[28] J. Quesada, L. Faba, E. Díaz, S. Ordóñez, Enhancement of the 1-butanol productivity in the ethanol condensation catalyzed by noble metal nanoparticles supported on Mg-Al mixed oxide, Appl. Catal. A: Gen. 563 (2018) 64–72.
[29] J. Quesada, L. Faba, E. Díaz, S. Ordóñez, Tuning the selectivities of Mg-Al mixed oxides for ethanol upgrading reactions through the presence of transition metals, Appl. Catal. A: Gen. 559 (2018) 167–174.
[30] Z. Liang, D. Jiang, G. Fang, W. Leng, P. Tu, Y. Tong, L. Liu, J. Ni, X. Li, Catalytic Enhancement of Aldol Condensation by Oxygen Vacancy on CeO2 Catalysts, ChemistrySelect 4 (2019) 4364–4370.
[31] S. Bhasker-Ranganath, M.S. Rahman, C. Zhao, F. Calaza, Z. Wu, Y. Xu, Elucidating the Mechanism of Ambient-Temperature Aldol Condensation of Acetaldehyde on Ceria, ACS Catal. 11 (2021) 8621–8634.
[32] J.H. Earley, R.A. Bourne, M.J. Watson, M. Poliakoff, Continuous catalytic upgrading of ethanol to n-butanol and >C4 products over Cu/CeO2 catalysts in supercritical CO_2, Green. Chem. 17 (2015) 3018–3025.
[33] D. Jiang, X. Wu, J. Mao, J. Ni, X. Li, Continuous catalytic upgrading of ethanol to n-butanol over Cu–CeO2/AC catalysts, Chem. Commun. 52 (2016) 13749–13752.
[34] D. Jiang, G. Fang, Y. Tong, X. Wu, Y. Wang, D. Hong, W. Leng, Z. Liang, P. Tu, L. Liu, K. Xu, J. Ni, X. Li, Multifunctional Pd@UiO-66 Catalysts for Continuous Catalytic Upgrading of Ethanol to n -Butanol, ACS Catal. 8 (2018) 11973–11978.
[35] J. Quesada, R. Arreola-Sánchez, L. Faba, E. Díaz, V.M. Rentería-Tapia, S. Ordóñez, Effect of Au nanoparticles on the activity of TiO2 for ethanol upgrading reactions, Appl. Catal. A: Gen. 551 (2018) 23–33.
[36] C. Yang, Z.Y. Meng, Bimolecular condensation of ethanol to 1-butanol catalyzed by alkali cation zeolites, J. Catal. 142 (1993) 37–44.
[37] K.W. Yang, X.Z. Jiang, W.C. Zhang, One-step synthesis of n-butanol from ethanol condensation over alumina-supported metal catalysts, Chin. Chem. Lett. 15 (2004) 1497–1500.
[38] J. Pasel, J. Häusler, D. Schmitt, H. Valencia, M. Meledina, J. Mayer, R. Peters, Ethanol Dehydrogenation: A React. Path Study Tempo Anal. Prod. 10 (2020) 1151.
[39] S. Brunauer, P.H. Emmett, E. Teller, Adsorption of gases in multimolecular layers, J. Am. Chem. Soc. 60 (1938) 309–319.
[40] C.L. Yaws, M.A. Satyro, Chapter 1 - Vapor Pressure – Organic Compounds, in: C.L. Yaws, (Ed.), The Yaws Handbook of Vapor Pressure (Second Edition), Gulf Professional Publishing, 2015, pp. 1–314.
[41] H. Shin, M. Choi, H. Kim, A mechanistic model for hydrogen activation, spillover, and its chemical reaction in a zeolite-encapsulated Pt catalyst, Phys. Chem. Chem. Phys. 18 (2016) 7035–7041.

[42] N. Yodsin, C. Rungnim, V. Promarak, S. Namuangruk, N. Kungwan, R. Rattanawan, S. Jungsuttiwong, Influence of hydrogen spillover on Pt-decorated carbon nanocones for enhancing hydrogen storage capacity: A DFT mechanistic study, Phys. Chem. Chem. Phys. 20 (2018) 21194–21203.
[43] H. Zhang, Y. Meng, G. Song, F. Li, Effect of hydrogen spillover to the hydrogenation of benzene over Pt/NaA catalysts, Synth. React. Inorg., Met. -Org. Nano-Met. Chem. 46 (2016) 940–944.
[44] H. Zhou, J. Zhang, D. Ji, A. Yuan, X. Shen, Effect of catalyst loading on hydrogen storage capacity of ZIF-8/graphene oxide doped with Pt or Pd via spillover, Microporous Mesoporous Mater. 229 (2016) 68–75.
[45] M.D. Driessen, V.H. Grassian, Methyl spillover on silica-supported copper catalysts from the dissociative adsorption of methyl halides, J. Catal. 161 (1996) 810–818.